The Astronomical Journal, 155:161 (15pp), 2018 April https://doi.org/10.3847/1538-3881/aab042

Robo-AO *Kepler* Survey. IV. The Effect of Nearby Stars on 3857 Planetary Candidate Systems

Carl Ziegler[1], Nicholas M. Law[1], Christoph Baranec[2], Reed Riddle[3], Dmitry A. Duev[3], Ward Howard[1], Rebecca Jensen-Clem[4], S. R. Kulkarni[3], Tim Morton[5], and Maïssa Salama[2]
[1] Department of Physics and Astronomy, University of North Carolina at Chapel Hill, Chapel Hill, NC 27599-3255, USA; carlziegler@unc.edu
[2] Institute for Astronomy, University of Hawai'i at Mānoa, Hilo, HI 96720-2700, USA
[3] Department of Astronomy, California Institute of Technology, 1200 East California Boulevard, Pasadena, CA 91101, USA
[4] University of California, Berkeley, 510 Campbell Hall, Astronomy Department, Berkeley, CA 94720, USA
[5] Department of Astrophysical Sciences, Princeton University, Princeton, NJ 08544, USA
Received 2017 December 11; revised 2018 February 12; accepted 2018 February 14; published 2018 March 21

Abstract

We present the overall statistical results from the Robo-AO *Kepler* planetary candidate survey, comprising of 3857 high-angular resolution observations of planetary candidate systems with Robo-AO, an automated laser adaptive optics system. These observations reveal previously unknown nearby stars blended with the planetary candidate host stars that alter the derived planetary radii or may be the source of an astrophysical false positive transit signal. In the first three papers in the survey, we detected 440 nearby stars around 3313 planetary candidate host stars. In this paper, we present observations of 532 planetary candidate host stars, detecting 94 companions around 88 stars; 84 of these companions have not previously been observed in high resolution. We also report 50 more-widely separated companions near 715 targets previously observed by Robo-AO. We derive corrected planetary radius estimates for the 814 planetary candidates in systems with a detected nearby star. If planetary candidates are equally likely to orbit the primary or secondary star, the radius estimates for planetary candidates in systems with likely bound nearby stars increase by a factor of 1.54, on average. We find that 35 previously believed rocky planet candidates are likely not rocky due to the presence of nearby stars. From the combined data sets from the complete Robo-AO KOI survey, we find that 14.5 ± 0.5% of planetary candidate hosts have a nearby star with 4″, while 1.2% have two nearby stars, and 0.08% have three. We find that 16% of Earth-sized, 13% of Neptune-sized, 14% of Saturn-sized, and 19% of Jupiter-sized planet candidates have detected nearby stars.

Key words: binaries: close – instrumentation: adaptive optics – methods: data analysis – methods: observational – planets and satellites: detection – techniques: high angular resolution

Supporting material: machine-readable tables

1. Introduction

Over its initial four-year mission, the *Kepler* telescope observed hundreds of thousands of stars, searching for the slight dip in brightness consistent with a transiting exoplanet. *Kepler* has exquisite photometric precision but relatively low spatial resolution, with an effective point-spread function (PSF) of 6″–10″ and a pixel size of ∼4″ (Haas et al. 2010). The majority of *Kepler* targets are solar-type (Batalha et al. 2013), and most form with at least one companion star (Duquennoy & Mayor 1991; Raghavan et al. 2010). These companion[6] stars are often blended with the planetary host star in the *Kepler* aperture, resulting in inaccurate host star characterization (Dressing & Charbonneau 2013; Santerne et al. 2013) and a high number of astrophysical false positive transit signals, estimated to be ∼10% of planetary candidates (Morton & Johnson 2011; Fressin et al. 2013). Even when the candidates are bona fide planets, the planet radius measurements based on the diluted transit signal are underestimated due to the presence of multiple stars in the system or unbounded stars within the *Kepler* photometric aperture (Morton & Johnson 2011). All planetary candidates discovered with light curves produced by *Kepler* must, therefore, be independently validated by ground-based high-angular resolution observations.

The challenge of performing high-angular resolution follow-up observations of the 4100 planet candidates (*Kepler* objects of interest, or KOIs) discovered by *Kepler* (Borucki et al. 2010, 2011a, 2011b; Batalha et al. 2013; Burke et al. 2014; Rowe et al. 2014; Coughlin et al. 2016; Morton et al. 2016; Mathur et al. 2017) has been met with considerable effort by the community (Howell et al. 2011; Adams et al. 2012, 2013; Horch et al. 2012, 2014; Lillo-Box et al. 2012, 2014; Dressing et al. 2014; Marcy et al. 2014; Everett et al. 2015; Gilliland et al. 2015; Torres et al. 2015; Wang et al. 2015a, 2015b; Kraus et al. 2016; Furlan et al. 2017). Many of these surveys were performed with large-aperture telescopes, sensitive to close (tens of mas separation) and faint (8–10 mag fainter than the host star) nearby stars. However, the combined efforts of surveys with traditional high-resolution instruments—in particular, adaptive optics—has resulted in a piecemeal approach, covering less than half of the KOIs. This is in part a result of redundant observations of a small set of KOIs, as the target lists of these surveys are often biased toward bright stars. This bias also results in a high fraction of early-type stars and stars closer to the Sun, which skews any interpretations drawn from the data. In addition, disparities in the instruments and passbands of these observations may lead to inconsistent vetting, as each survey has different detection sensitivities to nearby stars. The comprehensive statistics and correlations that can be derived from a homogeneous data set of thousands of high-resolution

[6] For brevity, we denote stars that we found within our detection radius of KOIs as "companions," in the sense that they are asterisms associated on the sky.

images of multiple stellar systems hosting planets are extremely difficult to obtain when using data from multiple surveys.

With an order-of-magnitude increase in observational time-efficiency compared to traditional systems provided by Robo-AO, the first fully automated laser adaptive optics system, we are performing high-resolution imaging of every KOI system to search for companions with separations between 0.″15 and 4.″0. The first paper in this survey, Law et al. (2014, hereafter Paper I), observed 715 *Kepler* planetary candidates, identifying 53 companions, with 43 new discoveries, for a detected companion fraction of 7.4% ± 1.0% within separations of 0.″15 to 2.″5. The second paper in this survey, Baranec et al. (2016, hereafter Paper II), observed 969 *Kepler* planetary candidates, identifying 202 companions, with 139 new discoveries, for a detected companion fraction of 11.0% ± 1.1% within separations of 0.″15 to 2.″5, and 18.1% ± 1.3% within separations of 0.″15 to 4.″0. The third paper, Ziegler et al. (2017, hereafter Paper III) in this survey observed 1629 KOIs, around which 223 companions were found around 206 KOIs, for a detected companion fraction of 12.6% ± 0.9% within 4.″0 of planetary candidate hosting stars.

This paper presents the detection of nearby stars from observations of 532 KOIs, and also expands the search for nearby stars around 715 KOIs observed initially in Paper I from its initial separation limit of 2.″5–4.″0. We also present the cumulative statistics from the survey, as well as derive corrected planetary radii for every candidate planet in a system with an observed nearby star.

We begin in Section 2 by describing our target selection, the Robo-AO system, and follow-up observations. In Section 3, we describe the Robo-AO data reduction and the companion detection and analysis. In Section 4, we describe the results of this survey, including discovered companions, and compare to other KOI surveys. We discuss the results in Section 5 and conclude in Section 6.

2. Survey Targets and Observations

2.1. Target Selection

The objective of the Robo-AO *Kepler* survey is to perform high-resolution observations of every KOI. We therefore targeted KOIs not observed in Paper I, Paper II, or Paper III from the *Kepler* DR25 catalog based on Q1-Q17 data (Borucki et al. 2010, 2011a, 2011b; Batalha et al. 2013; Burke et al. 2014; Rowe et al. 2014; Coughlin et al. 2016; Mathur et al. 2017). Observations of these targets presented in this paper are from the 2016 observing season. KOIs flagged as false positives using *Kepler* data were removed. In Figure 1, the properties of the targeted KOIs in this work as well as for the full Robo-AO survey as of the end of the 2016 observing season are compared to the set of all KOIs from Q1-Q17 with CANDIDATE dispositions based on *Kepler* data. The Robo-AO *Kepler* survey has observed more than 95% of KOIs, and the distribution of observed KOIs in the survey closely matches the full KOI list in magnitude, planetary radius, planetary orbital period, and stellar temperature.

To compile a homogeneous survey, the observations of 715 KOIs in Paper I were re-analyzed to search for companions between the 2.″5 separation limit implemented in that paper and the 4.″0 separation limit of Papers II and III. Observations of these targets were performed in the 2012 observing season.

2.2. Observations

We obtained high-angular-resolution images of 532 KOIs not previously observed by Robo-AO during 18 separate nights of observations between 2016 June 08 and 2016 July 15 (UT), detailed in Table 9 in the Appendix. The observations were performed using the Robo-AO laser adaptive optics system (Riddle et al. 2012; Baranec et al. 2013, 2014b) mounted on the Kitt Peak 2.1 m telescope (Jensen-Clem et al. 2017), masked to a 1.85 m aperture. The AO system runs at a loop rate of 1.2 kHz to correct high-order wavefront aberrations. Observations were taken in a long-pass filter cutting on at 600 nm (LP600 hereafter). The LP600 filter approximates the *Kepler* passband at redder wavelengths, while also suppressing blue wavelengths that reduce adaptive optics performance. The LP600 passband is compared to the *Kepler* passband in Figure 1 of Paper I.

Typical seeing at the Kitt Peak Observatory is between 0.″8 and 1.″6, with a median around 1.″3 (Jensen-Clem et al. 2017). The typical FWHM (diffraction limited) resolution of the Robo-AO system is 0.″15. Images are recorded on an electron-multiplying CCD (EMCCD), allowing short frame rates for tip and tilt correction in software using a natural guide star ($m_V < 16$) in the field of view. Specifications of the entire Robo-AO KOI survey are summarized in Table 2.

In addition to new observations, we also search for companions at wider separations from the Paper I target list, using observations taken with Robo-AO at Palomar Observatory. The description of these observations is available in Section 2.2 of Paper I, with the full target list available in Table 5 of Paper I.

3. Data Reduction

With a large adaptive optics data set acquired by Robo-AO, the data reduction process was automated as much as possible for efficiency and consistency. As in previous papers in the survey, after initial pipeline reductions described in Section 3.1, the target stars were identified (Section 3.2), PSF subtraction performed (Section 3.3), nearby stars identified by visual inspection and by an automated companion search algorithm (Section 3.4), and constraints of the nearby star sensitivity of the survey measured (Section 3.5). Finally, the properties of the detected companions are measured in Section 3.6.

3.1. Imaging Pipeline

The Robo-AO imaging pipeline (Law et al. 2009, 2014) reduced the images: the raw EMCCD output frames are dark-subtracted and flat-fielded and then stacked and aligned using the Drizzle algorithm (Fruchter & Hook 2002), which also up-samples the images by a factor of two. To avoid tip/tilt anisoplanatism effects, the image motion was corrected by using the KOI itself as the guide star in each observation.

3.2. Target Verification

To verify that the star viewed in the image is the desired KOI target, we created Digital Sky Survey and UKIRT (Lawrence et al. 2007) cut-outs of similar angular size around the target coordinates. Each image was manually checked to assure no ambiguity in the target star and images with either poor performance or incorrect fields were removed. These bad

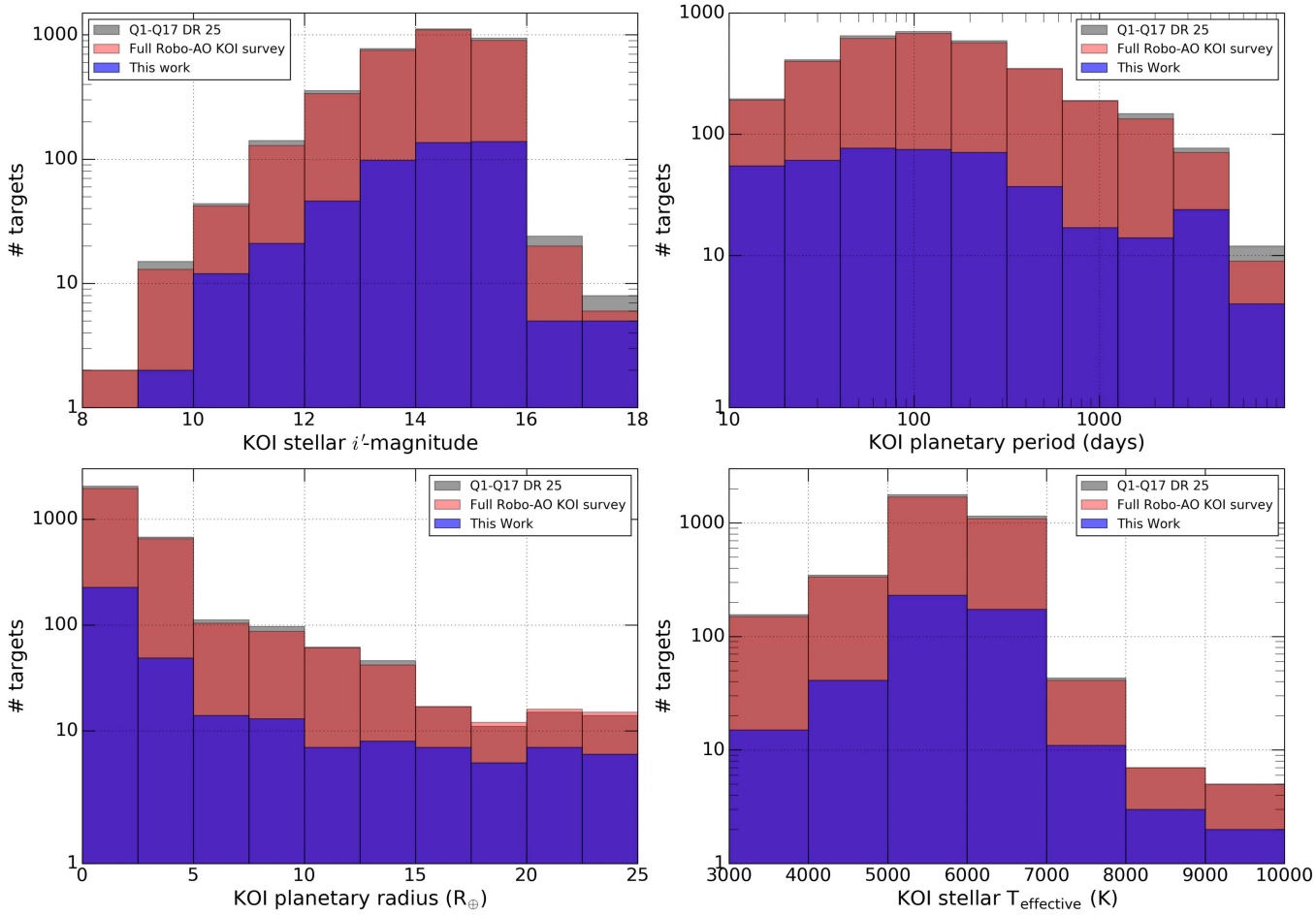

Figure 1. Comparison of the distribution of new Robo-AO observations in this paper as well as the combined Robo-AO survey (Paper I, Paper II, Paper III, and this work) to the complete set of KOIs from Q1-Q17 (Borucki et al. 2010, 2011a, 2011b; Batalha et al. 2013; Burke et al. 2014; Rowe et al. 2014; Coughlin et al. 2016; Mathur et al. 2017). Some observed KOIs with "CANDIDATE" disposition in early data releases that were observed with Robo-AO have been modified to "FALSE POSITIVE" in later releases, leading to a higher number of targets observed in some parameter bins, specifically at large planetary radii, than there are candidate systems in the latest *Kepler* data release.

images made up approximately 1% of all our images, and for all of the targets additional images were available.

We select a 4″ separation cut-off for our companion search to detect all nearby stars that would blend with the target KOI in a *Kepler* pixel. To facilitate the automation of the data reduction, centered 8.″5 square cut-outs were created around the 532 verified target KOIs, slightly larger than the diameter of our adopted separation limit so as to not remove a portion of the PSF of any nearby star within 4″.

3.3. PSF Subtraction

To identify close companions, a custom locally optimized PSF subtraction routine based on the Locally Optimized Combination of Images algorithm (Lafrenière et al. 2007) was applied to centered cut-outs of every star. The code uses a set of twenty KOI observations, selected from the observations within the same filter closest to the target observation in time, as reference PSFs. We address the potential that nearby stars will not be detected due to the use of other KOIs as reference images in Appendix A and find that no nearby stars are likely to be missed. A locally optimized PSF is generated and subtracted from the original image, leaving residuals consistent with photon noise. This procedure was performed on all KOI images out to a radius of 2″ from the host star. Figure 4 in Paper III shows an example of the PSF subtraction performance.

3.4. Companion Detection

An initial visual companion search on the original and PSF-subtracted images was performed redundantly by two of the authors. This search yielded a preliminary companion list and filtered out bad images.

Continuing the companion search, we ran all images through a custom automated search algorithm, based on the code described in Paper I. The algorithm slides a 5 pixel diameter aperture within concentric annuli centered on the target star. For each annulus, the mean and standard deviation of the local noise is estimated using the fluxes within these apertures, with a sigma clip employed to remove any anomalously high signals such as those arising from a real astrophysical source. Any aperture with a summed signal greater than $+5\sigma$ compared to the local noise is considered a potential astrophysical source. These are subsequently checked manually, eliminating spurious detections with dissimilar PSFs to the target star and those having characteristics of a cosmic ray hit, such as a single bright pixel or bright streak. The detection significance of detected companions are listed in Tables 3 and 1.

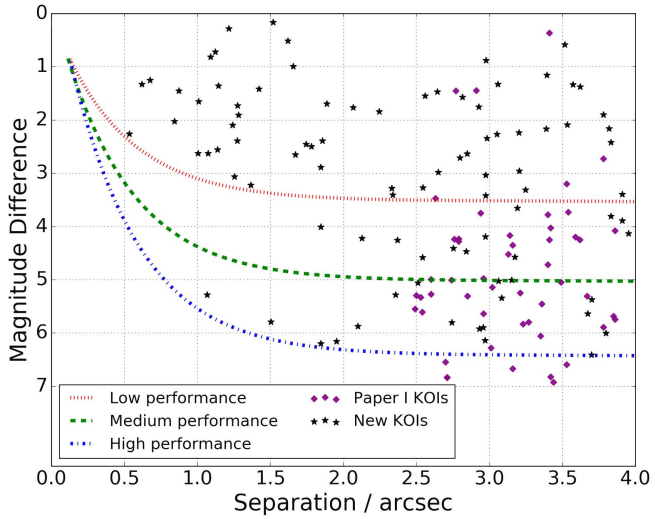

Figure 2. Separations and magnitude differences of the detected companions outside 2.″5 and within 4.″0 from the Paper I targets in black, and from new observations of previously unpublished KOIs in purple. Typical contrasts curves consistent with a 5σ detection on low-, medium- and high-performance images are plotted (as described in Section 3.5).

3.5. Imaging Performance Metrics

The two dominant factors that affect the image performance of the Robo-AO system are seeing and target brightness. An automated routine was used to classify the image performance for each target. The code uses PSF core size as a proxy for image performance. Observations were binned into three performance groups, with 31% fall in the low-performance group, 41% in the medium performance group, and 28% in the high-performance group.

We determine the angular separation and contrast consistent with a 5σ detection by injecting artificial companions, a clone of the primary PSF.[7] For concentric annuli of 0.″1 width, the detection limit is calculated by repeatedly dimming the artificial companion until the auto-companion detection algorithm (Section 3.4) fails to detect it. This process is subsequently performed at multiple random azimuths within each annulus, and the limiting 5σ magnitudes are averaged. For clarity, these average magnitudes for all radii measurements are fitted with functions of the form $a \times \sinh(b \times r + c) + d$ (where r is the radius from the target star and a, b, c and d are fitting variables). The limiting contrast curves from observations with Robo-AO at Palomar and Kitt Peak were determined and found to be similar. Typical contrast curves for the three performance groups are shown in Figure 5.

3.6. Nearby Star Properties

3.6.1. Contrast Ratios

For wide, resolved companions with little PSF overlap, the companion to primary star contrast ratio was determined using aperture photometry on the original images. The aperture radius was cycled in one-pixel increments from 1 to 5 FWHM for each system, with background measured opposite the primary from the companion (except in the few cases where another object falls near or within this region in the image). Photometric uncertainties are estimated from the standard deviation of the contrast ratios measured for the various aperture sizes.

For close companions, the estimated PSF was used to remove the blended contributions of each star before aperture photometry was performed. The locally optimized PSF subtraction algorithm can attempt to remove the flux from companions using other reference PSFs with excess brightness in those areas. For detection purposes, we use many PSF core sizes for optimization, and the algorithm's ability to remove the companion light is reduced. However, the companion is artificially faint as some flux has still been subtracted. To avoid this, the PSF fit was redone excluding a six-pixel-diameter region around the detected companion. The large PSF regions allow the excess light from the primary star to be removed, while not reducing the brightness of the companion.

3.6.2. Separation and Position Angles

Separation and position angles were determined from the raw pixel positions. Uncertainties were found using estimated systematic errors due to blending between components. Typical uncertainty in the position for each star was 1–2 pixels. Position angles and the plate scale for observations at Palomar were calculated using a distortion solution produced using Robo-AO measurements for the globular cluster M15.[8]

4. Discoveries

We observed 532 KOIs with Robo-AO, around which we find 94 companions nearby 88 KOIs. 84 of these KOIs with nearby stars have not been previously imaged in high resolution. We find a companion fraction of 16.7 ± 1.6% within 4.″0 of the 532 planetary candidate hosting stars. Cut-outs of all multiple star systems are shown in Figures 2 and 3, and measured properties of the systems are detailed in Table 1.

In addition, we find 50 additional companions outside 2.″5 and within 4.″0 around 48 KOIs from 715 targeted KOIs previously observed in Paper I. Combined with the nearby stars found within 2.″5 of the 715 KOIs in Paper I, we detect 103 stars nearby 96 KOIs, for a nearby star fraction rate of 13.4 ± 1.4%[9] within 4.″0 of a KOI. Cut-outs of the KOIs from Paper I with newly detected nearby stars are shown in Figure 6, and measured properties of the systems are detailed in Table 3.

The detected companion separations and contrast ratios of observed nearby stars to KOIs are plotted in Figure 5, along with the calculated 5σ detection limits as detailed in Section 3.5.

4.1. Comparison to Other Surveys

Some of the KOIs with observations presented in this paper have been previously observed in other surveys. In this section, we compare our nearby star detections and non-detections with the observations from other telescopes.

Lillo-Box et al. (2012, 2014) observed 98 and 174 KOIs, respectively, using the AstraLux Lucky Imaging system on the 2.2 m telescope at the Calar Alto Observatory. The nearby stars to KOI-99, 465, 626, 628, 644, 685, 1781, and 1812, all from

[7] We find that for Robo-AO data the companion injection method provides a more realistic measure of the detection sensitivity compared to mapping the contrasts consistent with a 5σ excursion from the background noise, which results in contrast curves artificially a half-magnitude or more deeper.

[8] S. Hildebrandt (2013, private communication).

[9] Error based on Poissonian statistics (Burgasser et al. 2003).

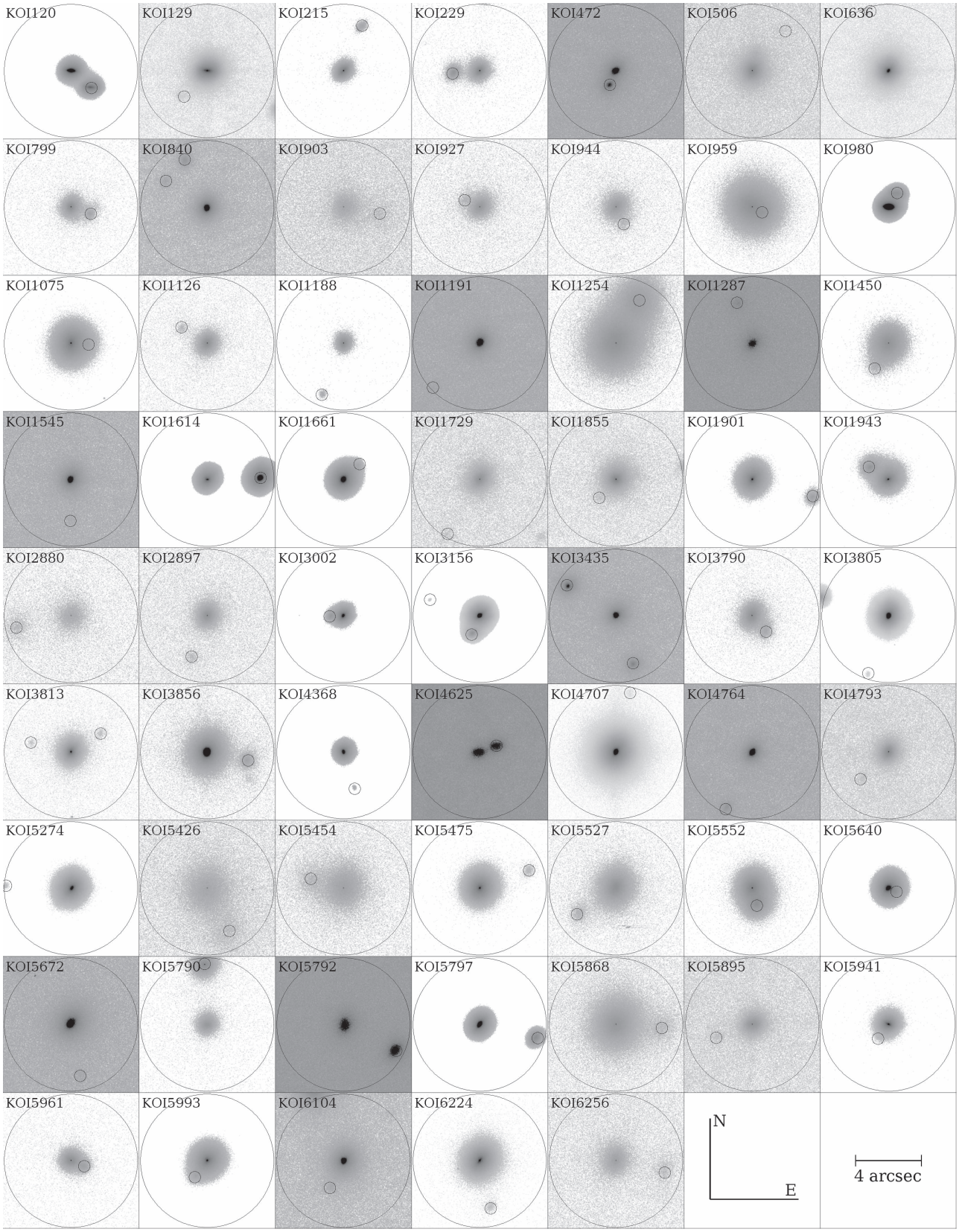

Figure 3. Color inverted, normalized log-scale cut-outs of 61 multiple KOI systems [KOI-120 to KOI-6256] resolved with Robo-AO from Kitt Peak. The angular scale and orientation are similar for each cut-out. The smaller circles are centered on the detected nearby star, and the larger circle is the limit of the survey's 4″ separation range.

the Paper I target list, were previously detected by them, as well as KOI-3805 from the targets observed with Robo-AO presented in this work. We did not detect the nearby star to KOI-238 from Lillo-Box et al. (2012) with $\Delta m_J = 4.38$; this star may be significantly fainter in the visible leading to our non-detection. We also do not detect the nearby stars from Lillo-Box et al.

Table 1
Detections of Objects Nearby 532 Previously Unpublished *Kepler* Planet Candidates

KOI	m_{Kep} (mag)	ObsID	Filter	Det. Significance σ	Separation ($''$)	P.A. (degree)	Mag. Diff. (mag)	Previous High Res.?
120	12.003	2016 Jul 15	LP600	7.3	1.62 ± 0.06	129 ± 2	0.51 ± 0.01	···
129	13.224	2016 Jul 15	LP600	6.7	2.1 ± 0.06	221 ± 3	5.87 ± 0.1	···
215	14.708	2016 Jul 14	LP600	11.1	2.98 ± 0.06	22 ± 2	2.34 ± 0.02	···
229	14.720	2016 Jun 17	LP600	6.2	1.66 ± 0.06	264 ± 2	0.99 ± 0.04	···
472	15.000	2016 Jun 18	LP600	7.2	1.12 ± 0.06	206 ± 2	0.72 ± 0.07	···
506	14.731	2016 Jun 18	LP600	4.5	3.15 ± 0.06	39 ± 4	5.0 ± 0.14	···
506	14.731	2016 Jun 18	LP600	13.2	1.13 ± 0.06	15 ± 3	3.35 ± 0.07	···
636	13.252	2016 Jun 17	LP600	60.1	3.8 ± 0.06	343 ± 5	6.0 ± 0.06	···
799	15.279	2016 Jun 16	LP600	7.4	1.28 ± 0.06	108 ± 2	1.73 ± 0.05	···
840	15.028	2016 Jun 17	LP600	5.4	2.97 ± 0.06	302 ± 3	3.42 ± 0.03	···
840	15.028	2016 Jun 17	LP600	11.9	3.2 ± 0.06	334 ± 2	2.24 ± 0.01	···
903	15.813	2016 Jun 27	LP600	5.1	2.24 ± 0.06	99 ± 2	1.84 ± 0.1	···
927	15.453	2016 Jul 08	LP600	4.8	1.01 ± 0.06	294 ± 3	2.63 ± 0.04	···
944	15.361	2016 Jul 08	LP600	5.7	1.14 ± 0.06	155 ± 2	2.55 ± 0.05	···
959	13.102	2016 Jun 25	LP600	5.5	0.68 ± 0.06	117 ± 4	1.25 ± 0.02	F17
980	10.376	2016 Jul 15	LP600	5.3	1.01 ± 0.06	31 ± 3	1.65 ± 0.03	F17
1075	13.056	2016 Jul 02	LP600	4.3	1.07 ± 0.06	93 ± 3	2.63 ± 0.07	···
1126	15.259	2016 Jun 19	LP600	8.1	1.85 ± 0.06	302 ± 2	2.89 ± 0.04	···
1188	15.381	2016 Jun 17	LP600	11.1	3.39 ± 0.06	202 ± 2	2.16 ± 0.02	···
1191	15.240	2016 Jun 17	LP600	8.6	3.91 ± 0.06	226 ± 3	3.89 ± 0.14	···
1254	12.777	2016 Jun 25	LP600	5.0	2.98 ± 0.06	28 ± 2	0.88 ± 0.05	···
1287	15.910	2016 Jun 18	LP600	8.4	2.64 ± 0.06	339 ± 2	1.47 ± 0.01	···
1450	13.480	2016 Jun 25	LP600	5.4	1.74 ± 0.06	208 ± 2	2.46 ± 0.04	···
1545	15.169	2016 Jun 18	LP600	4.3	2.51 ± 0.06	180 ± 4	5.06 ± 0.18	···
1614	11.413	2016 Jun 18	LP600	8.7	3.37 ± 0.06	87 ± 2	−0.44 ± 0.06	F17
1661	11.510	2016 Jun 18	LP600	7.0	1.37 ± 0.06	46 ± 2	3.22 ± 0.08	···
1729	15.424	2016 Jun 22	LP600	10.2	3.83 ± 0.06	210 ± 3	3.81 ± 0.07	···
1855	14.782	2016 Jun 17	LP600	4.7	1.5 ± 0.06	222 ± 4	5.79 ± 0.73	···
1901	13.340	2016 Jun 15	LP600	20.2	3.82 ± 0.06	105 ± 2	2.16 ± 0.02	···
1943	13.377	2016 Jun 22	LP600	7.2	1.42 ± 0.06	302 ± 3	1.42 ± 0.03	···
2880	15.918	2016 Jul 02	LP600	6.8	3.39 ± 0.06	257 ±	1.15 ± 0.12	···
2897	15.361	2016 Jun 18	LP600	8.4	2.65 ± 0.06	200 ± 2	2.98 ± 0.04	···
3002	13.256	2016 Jun 17	LP600	5.8	0.84 ± 0.06	267 ± 4	2.02 ± 0.05	···
3156	7.899	2016 Jun 17	LP600	9.5	1.24 ± 0.06	203 ± 2	2.09 ± 0.03	F17
3156	7.899	2016 Jun 17	LP600	15.8	3.06 ± 0.06	288 ± 3	5.02 ± 0.06	···
3435	15.259	2016 Jun 16	LP600	6.7	3.06 ± 0.06	160 ± 2	1.33 ± 0.02	···
3435	15.259	2016 Jun 16	LP600	14.9	3.52 ± 0.06	301 ± 2	0.58 ± 0.04	···
3790	18.590	2016 Jun 22	LP600	6.5	1.28 ± 0.06	138 ± 3	1.91 ± 0.05	···
3805	11.356	2016 Jun 17	LP600	3.8	3.7 ± 0.06	199 ± 4	5.37 ± 0.02	L12
3813	14.113	2016 Jun 18	LP600	10.3	2.54 ± 0.06	283 ± 3	4.58 ± 0.07	···
3813	14.113	2016 Jun 18	LP600	7.8	2.13 ± 0.06	58 ± 4	4.22 ± 0.02	···
3856	13.493	2016 Jun 16	LP600	8.2	2.54 ± 0.06	101 ± 2	3.27 ± 0.02	···
4368	13.046	2016 Jun 18	LP600	12.3	2.33 ± 0.06	162 ± 3	3.28 ± 0.01	···
4625	15.877	2016 Jul 15	LP600	7.0	1.22 ± 0.06	69 ± 3	0.28 ± 0.02	···
4707	11.660	2016 Jun 15	LP600	11.4	3.7 ± 0.06	13 ± 2	6.41 ± 0.03	···
4764	15.809	2016 Jun 19	LP600	24.2	3.83 ± 0.06	204 ± 2	2.42 ± 0.04	···
4793	15.374	2016 Jun 19	LP600	5.6	2.37 ± 0.06	225 ± 4	4.25 ± 0.09	···
5274	12.746	2016 Jun 22	LP600	5.4	3.95 ± 0.06	272 ± 3	4.13 ± 0.01	···
5426	13.701	2016 Jun 25	LP600	4.8	2.93 ± 0.06	152 ± 2	1.75 ± 0.11	···
5454	14.150	2016 Jun 25	LP600	4.5	2.07 ± 0.06	286 ± 2	1.77 ± 0.05	···
5475	13.093	2016 Jun 27	LP600	9.1	3.19 ± 0.06	70 ± 3	3.65 ± 0.01	F17
5527	14.174	2016 Jul 02	LP600	9.3	2.85 ± 0.06	236 ± 2	2.63 ± 0.01	···
5552	13.344	2016 Jun 27	LP600	4.8	1.09 ± 0.06	165 ± 3	0.82 ± 0.04	···
5640	12.038	2016 Jun 28	LP600	5.2	0.53 ± 0.06	113 ± 4	2.26 ± 0.05	···
5672	14.333	2016 Jul 08	LP600	10.1	3.17 ± 0.06	169 ± 3	4.58 ± 0.19	···
5790	15.518	2016 Jun 28	LP600	8.9	3.69 ± 0.06	357 ± 2	−0.67 ± 0.01	···
5792	15.705	2016 Jul 13	LP600	11.1	3.59 ± 0.06	116 ± 2	−0.07 ± 0.07	···
5797	12.220	2016 Jul 13	LP600	13.6	3.62 ± 0.06	103 ± 2	1.37 ± 0.05	···
5868	13.787	2016 Jul 02	LP600	3.5	2.8 ± 0.06	94 ± 2	2.71 ± 0.09	···
5895	15.337	2016 Jul 15	LP600	6.5	2.34 ± 0.06	249 ± 2	3.41 ± 0.03	···
5941	13.783	2016 Jul 13	LP600	6.7	1.07 ± 0.06	216 ± 4	5.28 ± 0.22	···
5961	15.053	2016 Jul 13	LP600	6.9	0.87 ± 0.06	112 ± 3	1.45 ± 0.03	···
5993	12.873	2016 Jun 14	LP600	7.8	1.25 ± 0.06	217 ± 3	3.06 ± 0.04	···

Table 1
(Continued)

KOI	m_{Kep} (mag)	ObsID	Filter	Det. Significance σ	Separation ($''$)	P.A. (degree)	Mag. Diff. (mag)	Previous High Res.?
6104	14.708	2016 Jun 16	LP600	8.7	1.84 ± 0.06	206 ± 3	4.01 ± 0.01	···
6224	12.962	2016 Jul 13	LP600	9.0	2.97 ± 0.06	167 ± 2	4.19 ± 0.01	···
6256	15.729	2016 Jun 15	LP600	6.8	3.05 ± 0.06	103 ± 2	2.27 ± 0.05	···
6297	14.043	2016 Jun 16	LP600	10.1	2.56 ± 0.06	103 ± 2	1.55 ± 0.01	···
6297	14.043	2016 Jun 16	LP600	6.3	2.96 ± 0.06	308 ± 5	5.89 ± 0.24	···
6384	15.992	2016 Jun 16	LP600	13.1	3.53 ± 0.06	285 ± 2	2.09 ± 0.01	···
6390	13.961	2016 Jun 17	LP600	10.9	2.82 ± 0.06	309 ± 2	1.57 ± 0.03	···
6600	10.715	2016 Jun 17	LP600	15.2	2.36 ± 0.06	315 ± 4	5.28 ± 0.02	F17
6697	13.678	2016 Jun 22	LP600	30.7	3.91 ± 0.06	313 ± 3	3.4 ± 0.01	···
6783	15.472	2016 Jun 22	LP600	5.5	3.25 ± 0.06	178 ± 3	3.31 ± 0.06	···
6793	14.835	2016 Jun 22	LP600	4.8	2.84 ± 0.06	309 ± 4	4.47 ± 0.25	···
6835	13.903	2016 Jun 22	LP600	8.2	3.08 ± 0.06	78 ± 5	5.34 ± 0.07	···
6907	15.930	2016 Jun 22	LP600	15.1	3.35 ± 0.06	99 ± 2	−0.36 ± 0.07	···
6918	14.596	2016 Jun 22	LP600	5.2	0.62 ± 0.06	98 ± 4	1.33 ± 0.04	···
7002	14.991	2016 Jun 27	LP600	6.2	3.2 ± 0.06	247 ± 2	2.95 ± 0.06	···
7003	14.106	2016 Jun 25	LP600	4.8	3.78 ± 0.06	285 ± 2	1.9 ± 0.09	···
7032	12.646	2016 Jun 22	LP600	4.1	2.74 ± 0.06	182 ± 4	5.8 ± 0.13	F17
7050	13.506	2016 Jun 27	LP600	5.3	1.78 ± 0.06	129 ± 2	2.5 ± 0.01	···
7087	12.457	2016 Jul 02	LP600	5.1	1.89 ± 0.06	165 ± 2	1.69 ± 0.02	···
7129	13.839	2016 Jun 28	LP600	6.2	1.27 ± 0.06	191 ± 2	2.39 ± 0.02	···
7220	15.102	2016 Jul 12	LP600	9.9	3.57 ± 0.06	27 ± 2	1.33 ± 0.07	···
7389	12.148	2016 Jul 14	LP600	9.8	1.84 ± 0.06	291 ± 6	6.2 ± 0.04	···
7408	15.949	2016 Jul 14	LP600	5.8	1.67 ± 0.06	184 ± 2	2.65 ± 0.06	···
7455	11.419	2016 Jul 08	LP600	6.1	1.86 ± 0.06	306 ± 3	2.39 ± 0.03	F17
7470	13.870	2016 Jul 15	LP600	6.4	1.52 ± 0.06	303 ± 2	0.17 ± 0.02	F17
7501	11.308	2016 Jul 15	LP600	5.6	1.15 ± 0.06	15 ± 2	1.36 ± 0.06	···
7527	13.573	2016 Jul 15	LP600	6.4	2.75 ± 0.06	98 ± 4	4.41 ± 0.06	···
7539	14.813	2016 Jul 15	LP600	7.3	2.97 ± 0.06	348 ± 3	3.03 ± 0.03	···
7540	13.852	2016 Jul 14	LP600	8.5	3.67 ± 0.06	152 ± 4	5.64 ± 0.06	···
7546	12.667	2016 Jun 17	LP600	6.7	2.93 ± 0.06	223 ± 5	5.92 ± 0.07	···
7572	9.748	2016 Jun 22	LP600	7.5	2.97 ± 0.06	16 ± 4	5.14 ± 0.01	···

Note. References for previous high-resolution observations are denoted using the following codes: Lillo-Box et al. (2012) (L12), Furlan et al. (2017) (F17).

(2014) to KOI-1230 ($\Delta m_{i'} = 9.11$) and KOI-2324 ($\Delta m_{i'} = 6.12$), which are outside our detection sensitivity.

Wang et al. (2015a) observed 84 KOIs using the PHARO and NIRC2 instruments at Palomar and Keck, respectively. We observe nearby stars to KOI-1692, 1781, and 2169 which they previously detected, but do not observe their detected nearby stars to KOI-344 ($\Delta m_J = 5.52$), KOI-1353 ($\Delta m_J = 4.87$), KOI-5515 ($\Delta m_J = 4.10$ and $\Delta m_J = 5.40$). The NIR photometry of the nearby stars to KOI-344 and 5515 suggest they are later spectral types than the target star and may be faint in the visible. The apparent visual magnitude of the nearby star to KOI-1353 is not known, and it may be too faint for detection in this survey.

Adams et al. (2012, 2013) observed 87 and 13 KOIs with the instruments ARIES and PHARO on the MMT and Palomar telescopes, respectively. We observe the nearby stars to KOI-75, 263, and 268 at separations greater than $2''.5$ which they had previously detected. They detect nearby stars to KOI-10, 18, 113, 1316, all with $\Delta m_J > 6.0$, which we did not detect as they likely have contrast ratios in the visible outside our detection sensitivity.

Observing 87 KOIs with ARIES at the MMT, Dressing et al. (2014) previously detected a nearby star to KOI-1279. In addition, they detected nearby stars to KOI-720 ($\Delta m_J = 5.50$) and KOI-2331 ($\Delta m_J = 4.55$), which we did not detect. NIR photometry suggests these nearby stars are redder than the target star, making them too faint for our survey to detect.

Table 2
The Specifications of the Robo-AO KOI Survey

KOI targets	3857
FWHM resolution	$\sim 0''.15$ (@600–750 nm)
Observation wavelengths	600–950 nm
Detector format	1024^2 pixels
Pixel scale	43 mas pix^{-1} (Palomar)
	35 mas pix^{-1} (Kitt Peak)
Exposure time	90 s
Targets observed/hour	20
Observation dates	2012 July 16 –
at Palomar	2015 June 12
Observation dates	2016 June 8 –
at Kitt Peak	2016 July 15

Gilliland et al. (2015) detected a nearby star to KOI-2650 ($\Delta m_{755W} = 7.55$) using the *Hubble Space Telescope*, too faint for detection in this survey.

Kraus et al. (2016) observed 382 KOIs with AO on the Keck II telescope. We observe nearby stars they previously detected to KOI-44, 70, 75, 99, 102, 148, 161, 214, 263, 268, 663, 701, 1692, 1781, 2169, and 2287. They detect faint ($\Delta m_K > 6.0$) stars, below our detection sensitivity, at separations outside $2''.5$ to Paper I targets: KOI-2, 41, 84, 85, 103, 105, 144, 152, 157, 177, 254, 261, 269, 372, 571, 701, 886, 899, 947, 1146, 1230, 1241, 1316, 1408, 1589, 1615, 1618, 1738, 1843, 2158, 2332, and 2593. They

Table 3
Detections of Objects Outside 2.″5 and within 4.″0 of *Kepler* Planet Candidates from Paper I Targets

KOI	m_{Kep} (mag)	ObsID	Filter	Det. Significance σ	Separation (″)	P.A. (degree)	Mag. Diff. (mag)	Previous High Res.?
44	13.483	2012 Jul 16	*i*	8.8	3.42 ± 0.06	123 ± 3	4.03 ± 0.04	K16
70	12.498	2012 Jul 16	*i*	20.6	3.86 ± 0.06	51 ± 4	5.74 ± 0.14	K16
75	10.775	2013 Aug 14	LP600	15.9	3.53 ± 0.06	124 ± 4	6.6 ± 0.03	A12, K16
99	12.960	2013 Jul 29	LP600	9.1	3.67 ± 0.06	46 ± 3	5.31 ± 0.03	K16, L12
102	12.566	2013 Oct 25	LP600	15.4	2.91 ± 0.06	221 ± 2	1.45 ± 0.01	···
107	12.702	2012 Jul 16	*i*	6.9	2.6 ± 0.06	273 ± 3	5.27 ± 0.08	···
148	13.040	2012 Jul 17	*i*	6.6	2.54 ± 0.06	245 ± 4	4.99 ± 0.06	K16
161	13.341	2012 Jul 18	LP600	18.2	2.7 ± 0.06	172 ± 5	6.55 ± 0.14	K16
162	13.837	2012 Jul 18	LP600	17.9	3.23 ± 0.06	0 ± 4	5.83 ± 0.09	···
214	14.256	2012 Jul 18	LP600	13.5	3.85 ± 0.06	119 ± 4	5.68 ± 0.07	K16
220	14.236	2012 Sep 01	LP600	8.3	3.13 ± 0.06	213 ± 3	4.52 ± 0.04	···
237	14.176	2012 Jul 18	LP600	5.5	3.16 ± 0.06	208 ± 4	6.67 ± 0.26	···
250	15.473	2012 Aug 03	LP600	3.0	3.44 ± 0.06	275 ± 3	6.92 ± 0.66	···
263	10.821	2012 Jul 18	*i*	19.0	3.34 ± 0.06	267 ± 2	0.59 ± 0.0	A12, K16
268	10.560	2012 Sep 14	LP600	9.0	2.50 ± 0.06	308 ± 3	5.55 ± 0.01	A12, K16
317	12.885	2012 Jul 28	*i*	10.5	3.02 ± 0.06	283 ± 3	5.14 ± 0.06	···
385	13.435	2012 Aug 02	*i*	9.0	3.36 ± 0.06	171 ± 2	5.45 ± 0.12	···
465	14.188	2012 Aug 05	LP600	12.1	3.62 ± 0.06	130 ± 3	4.25 ± 0.07	L12
486	14.118	2012 Aug 05	LP600	13.1	3.53 ± 0.06	71 ± 2	3.2 ± 0.03	···
509	14.883	2012 Sep 01	LP600	5.0	2.79 ± 0.06	305 ± 3	4.28 ± 0.14	···
509	14.883	2012 Sep 01	LP600	7.6	2.94 ± 0.06	55 ± 2	3.75 ± 0.04	···
568	14.140	2012 Aug 05	LP600	8.8	3.16 ± 0.06	142 ± 3	4.35 ± 0.05	···
626	13.490	2012 Aug 03	*i*	5.4	2.85 ± 0.06	349 ± 3	5.31 ± 0.04	L12
628	13.946	2012 Aug 03	*i*	8.1	2.76 ± 0.06	237 ± 4	4.24 ± 0.06	L12, F17
644	13.725	2012 Aug 04	*i*	32.2	2.77 ± 0.06	62 ± 3	1.45 ± 0.01	L12
650	13.594	2012 Aug 04	*i*	21.2	2.63 ± 0.06	269 ± 2	3.47 ± 0.07	L14, K16
663	13.506	2012 Sep 02	LP600	12.5	3.21 ± 0.06	61 ± 3	5.8 ± 0.09	K16
685	13.949	2013 Jul 27	LP600	33.5	3.35 ± 0.06	268 ± 5	6.05 ± 0.12	L12
701	13.725	2012 Aug 05	*i*	7.1	2.96 ± 0.06	105 ± 3	4.98 ± 0.06	K16, F17
1198	15.319	2012 Sep 03	LP600	5.0	3.11 ± 0.06	98 ± 4	5.25 ± 0.33	···
1279	13.749	2012 Aug 06	*i*	6.1	2.74 ± 0.06	134 ± 3	5.0 ± 0.1	D14
1366	15.368	2012 Sep 04	LP600	10.4	3.4 ± 0.06	119 ± 3	4.72 ± 0.18	···
1627	15.767	2012 Sep 04	LP600	27.9	3.41 ± 0.06	87 ± 2	0.37 ± 0.01	···
1692	12.557	2012 Aug 29	*i*	7.7	3.19 ± 0.06	342 ± 4	6.82 ± 0.13	W15, K16
1781	12.231	2012 Sep 13	LP600	13.6	3.4 ± 0.06	331 ± 3	3.78 ± 0.01	L12, W15, K16
1812	13.742	2012 Aug 29	*i*	5.7	2.71 ± 0.06	111 ± 5	6.84 ± 1.58	L12
1820	13.530	2012 Sep 13	LP600	37.9	3.78 ± 0.06	180 ± 4	5.89 ± 0.08	···
1845	14.438	2013 Oct 25	LP600	19.1	3.04 ± 0.06	347 ± 3	4.59 ± 0.09	···
1884	15.462	2012 Sep 13	LP600	5.8	2.54 ± 0.06	328 ± 4	5.61 ± 0.47	B16
1922	15.356	2012 Sep 13	LP600	24.5	3.78 ± 0.06	195 ± 2	2.73 ± 0.03	···
2022	14.746	2012 Sep 13	LP600	10.4	3.14 ± 0.06	71 ± 3	4.16 ± 0.13	···
2022	14.746	2012 Sep 13	LP600	7.8	2.5 ± 0.06	152 ± 3	5.3 ± 0.26	···
2025	13.781	2012 Sep 13	LP600	15.9	3.49 ± 0.06	191 ± 4	5.05 ± 0.02	···
2105	13.862	2012 Oct 06	LP600	7.6	3.01 ± 0.06	314 ± 3	5.28 ± 0.11	···
2169	12.404	2012 Aug 31	*i*	30.1	3.59 ± 0.06	66 ± 3	4.2 ± 0.01	W15, K16
2222	12.963	2012 Aug 31	*i*	6.1	2.53 ± 0.06	333 ± 3	5.33 ± 0.1	···
2287	12.485	2012 Aug 31	*i*	9.8	2.96 ± 0.06	11 ± 4	5.64 ± 0.09	K16
2547	14.169	2012 Oct 06	LP600	13.7	2.79 ± 0.06	151 ± 3	4.23 ± 0.02	···
2556	14.050	2012 Oct 06	LP600	17.7	3.86 ± 0.06	238 ± 2	4.08 ± 0.05	···
2582	13.628	2012 Aug 31	*i*	12.3	3.41 ± 0.06	223 ± 2	4.25 ± 0.05	···
2641	13.845	2012 Oct 06	LP600	17.9	3.54 ± 0.06	0 ± 2	3.73 ± 0.01	···

Note. References for previous high-resolution observations are denoted using the following codes: Adams et al. (2012) (A12), Lillo-Box et al. (2012) (L12), Dressing et al. (2014) (D14), Kraus et al. (2016) (K16), Wang et al. (2015a) (W16), Baranec et al. (2016) (B16), Furlan et al. (2017) (F17).

also detect faint nearby stars to KOI-72, 2650, and 2792 that were also observed with Robo-AO and presented in this work. These high-contrast stars are outside of our detection sensitivity.

Furlan et al. (2017) observed 253, 317, and 310 unique KOI host stars at Keck, Palomar, and Lick Observatory, respectively. We observe nearby stars previously detected by Furlan et al. (2017) to KOI-628, 701, 959, 980, 1614, 3156, 5475, 6600, 7032, 7455, and 7470.

We also detect the nearby star to KOI-1884 discovered with Keck-AO in Paper II.

In summary, we detect every star discovered by other surveys near the observed KOIs that have separations and

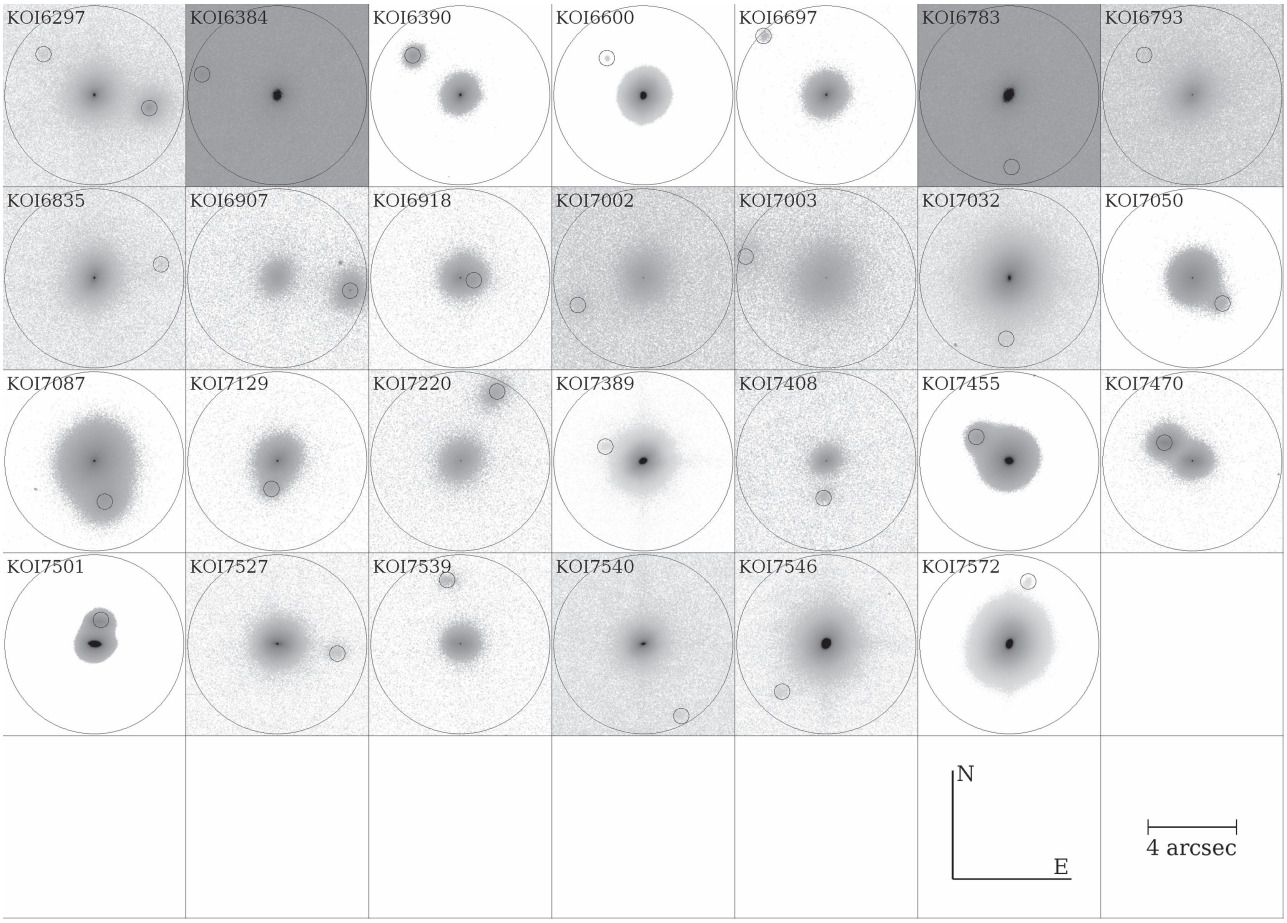

Figure 4. Color inverted, normalized log-scale cut-outs of 27 multiple KOI systems [KOI-6297 to KOI-7572] resolved with Robo-AO from Kitt Peak. The angular scale and orientation are similar for each cut-out. The smaller circles are centered on the detected nearby star, and the larger circle is the limit of the survey's 4″ separation range.

contrasts within our detection sensitivities. Many previous surveys were performed with large-aperture telescopes in the NIR, sensitive to faint and red companions, which we do not detect in this survey. If there is a true planet hosted by the primary star in the system, the flux from these nearby stars will have a negligible effect on the visible *Kepler* light curves.

5. Discussion

In this section, we present comprehensive statistics for the Robo-AO *Kepler* survey, as well as discuss the impact of the detected nearby stars on the planetary candidate properties.

5.1. Robo-AO KOI Survey Cumulative Statistics

The Robo-AO KOI survey has observed 3857 KOIs in Paper I, II, III, and this work. We find 610 nearby stars around 559 planetary candidate hosts in the combined survey data set, implying a nearby star fraction rate of 14.5 ± 0.6% within the Robo-AO detectability range (separations between ∼0.″15 and 4.″0 and $\Delta m \leqslant 6$). We also find within 4.″0 separation, a triple star fraction of 1.2 ± 0.2% and a quadruple star fraction of $0.08^{+0.06}_{-0.03}$%. The nearby star fraction rate as a function of separation from the host star for the survey to date is listed in Table 4 and plotted in Figure 4. The nearby star fraction increases linearly with separation from the host star. If all nearby stars were unbound, we would expect the rate to increase with the area enclosed. This suggests that a significant fraction of the nearby stars may be bound to the host star. It should be noted that this analysis does not account for the detection sensitivity of Robo-AO at varying separations. It is expected, however, that most nearby stars at separations <1″ are likely bound (Horch et al. 2014). We will assess the probability of association of individual systems in future papers in this survey.

The properties of planetary systems in binary star systems may be impacted due to perturbations from the secondary star. We show in Table 5 the nearby star fraction for different planet types based on their similarity in radius to a solar system planet. We find that the nearby star rates for all four planet types are within 2σ of the total rate for the entire survey. The largest outlier rate is for the Jupiter or gas giant planets, which are known to have a large false positive fraction (Santerne et al. 2013), caused by the potential of background eclipsing binaries to mimic their deep transits. Wang et al. (2014) also find a high stellar multiplicity rate for hot Jupiters, and direct imaging surveys find that gas giants have a high rate of bound stellar companions (Evans et al. 2016; Ngo et al. 2016). It is also possible that the high nearby star rate may be due to orbital migration caused by a bound secondary star that drives gas giants to low-period orbits more easily detectable by *Kepler*. In Paper III, we found a significant increase in the nearby star rate

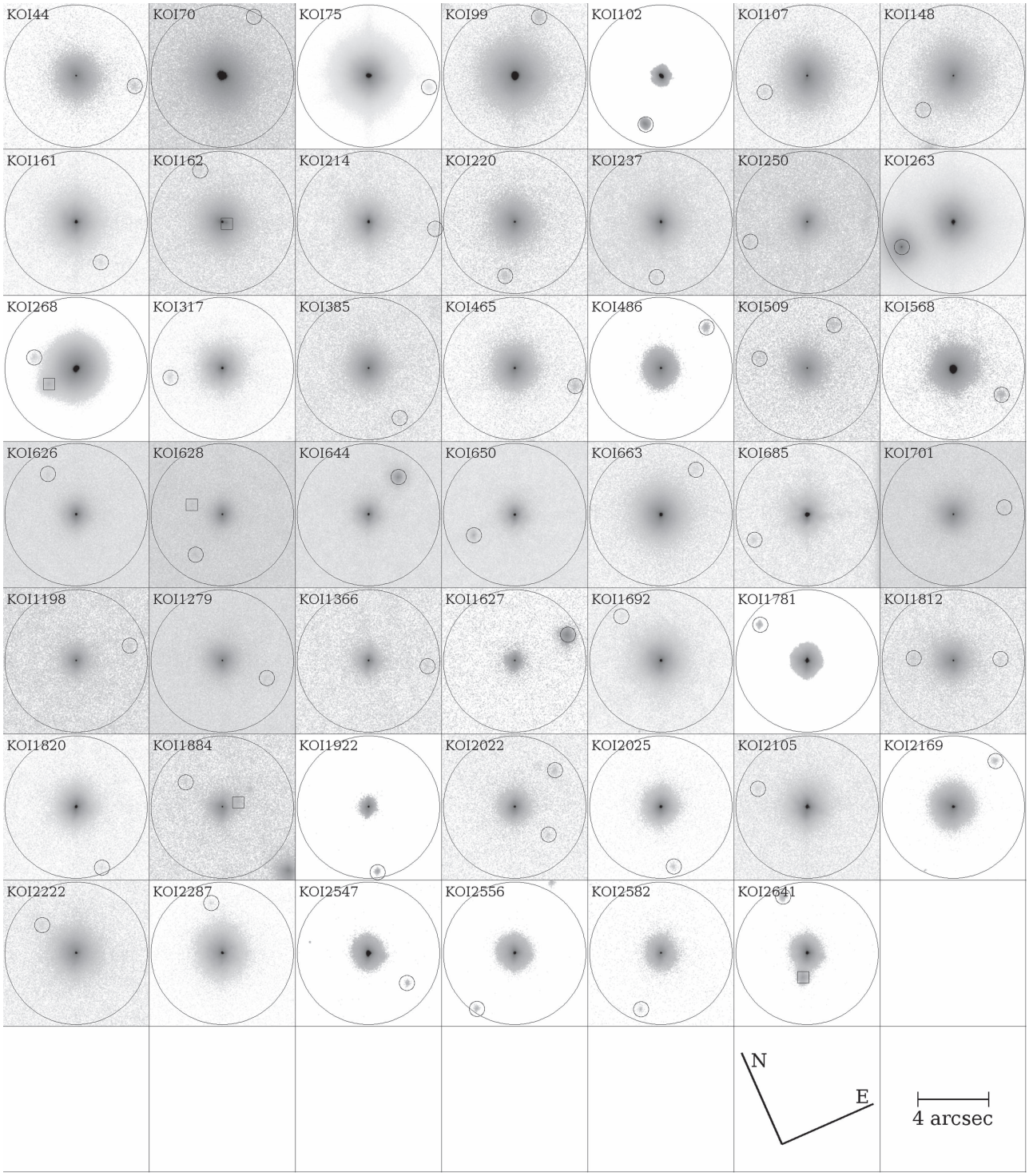

Figure 5. Color inverted, normalized log-scale cut-outs of 48 multiple KOI systems with separations outside 2.″5 and within 4″ resolved with Robo-AO at Palomar from the Paper I target list. The angular scale and orientation are similar for each cut-out. The smaller circles are centered on the detected nearby star, and the larger circle is the limit of the survey's 4″ separation range. Squares are centered on companions with separations less than 2.″5 found in Paper I from Robo-AO at Palomar.

for low-period giant planets, possibly caused by orbital migration due to the secondary star (Fabrycky & Tremaine 2007), although the significance of this effect may be small (Naoz et al. 2012; Petrovich 2015). These migrations may also cause planet scattering, differentially ejecting smaller planets from the system (Rasio & Ford 1996; Wang et al. 2015a).

5.2. *Implications for* Kepler *Planet Candidates*

A nearby star in the same photometric aperture as the target star will dilute the observed transit depth, resulting in underestimated radius estimates. We re-derive the estimated planetary radii for the 814 planetary candidates around the 559 KOIs with detected nearby stars in the Robo-AO *Kepler* survey

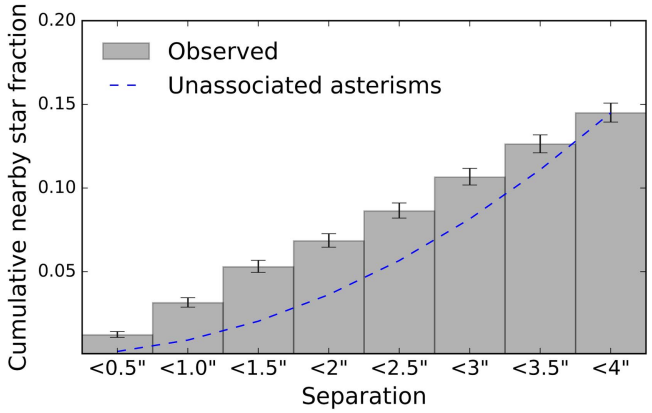

Figure 6. The nearby star fraction rate as a function of separation from 3857 observations of planetary candidates in the Robo-AO KOI survey. The dashed line represents a cumulative distribution that scales with the area that would be expected from non-physically associated companions.

Table 4
Robo-AO KOI Survey Cumulative Nearby Star Fraction Rates

Separation (″)	Systems with Nearby Stars	Nearby Star Rate[a] (%)
<0.5	47	$1.2^{+0.20}_{-0.15}$
<1.0	121	$3.1^{+0.30}_{-0.26}$
<1.5	204	$5.3^{+0.38}_{-0.33}$
<2.0	264	$6.8^{+0.43}_{-0.38}$
<2.5	333	$8.6^{+0.47}_{-0.43}$
<3.0	411	$10.7^{+0.52}_{-0.48}$
<3.5	487	$12.6^{+0.55}_{-0.52}$
<4.0	559	$14.5^{+0.59}_{-0.55}$

Note.
[a] Error based on Poissonian statistics (Burgasser et al. 2003).

Table 5
Nearby Star Fraction Rates by Planet Candidate Type

Planet Candidate Type	Planetary Radius Range	Systems with Nearby Stars	Total Systems	Nearby Star Rate
Earths	$R_p < 1.6R_\oplus$	241	1480	16.3 ± 1.0%
Neptunes	$1.6\,R_\oplus < R_p < 3.9\,R_\oplus$	268	2058	13.0 ± 0.8%
Saturns	$3.9\,R_\oplus < R_p < 9\,R_\oplus$	46	338	13.6 ± 2.0%
Jupiters	$9\,R_\oplus < R_p$	47	247	19.0 ± 2.8%

for two scenarios: (1) the planet orbits the target star; and (2) the planet orbits the secondary star which is bound to the primary star.[10] For the first case, we use the relation from Paper I to correct for the transit dilution,

$$R_{p,A} = R_{p,0}\sqrt{\frac{1}{F_A}} \quad (1)$$

where $R_{p,A}$ is the corrected radius of the planet orbiting the primary star, $R_{p,0}$ is the original planetary radius estimate based on the diluted transit signal, and F_A is the fraction of flux within the aperture from the primary star. For the case where the planet candidate is bound to the secondary star, we use the relation

$$R_{p,B} = R_{p,0}\frac{R_B}{R_A}\sqrt{\frac{1}{F_B}} \quad (2)$$

where $R_{p,B}$ is the corrected radius of the planet orbiting the secondary star bound to the primary star, R_B and R_A are the stellar radii of the secondary and primary star, respectively, and F_B is the fraction of flux within the aperture from the secondary star.

We use the stellar radius estimates from Mathur et al. (2017) for the primary stars. The radii of secondary companions in the scenario where they are bound to the target star were estimated using the observed contrast ratio in the *Kepler* band (approximated using the LP600 bandpass) and finding the radius of an appropriately fainter star within the Dartmouth stellar models (Dotter et al. 2008). The fluxes of all observed sources within the *Kepler* aperture were summed to estimate the transit dilution. The revised planetary radius estimates are detailed in Table 8.

The original derived planetary candidate radius estimates are corrected for dilution only from nearby stars resolved in the KIC (Coughlin et al. 2016). We find that four of the nearby stars detected in our survey appear in the KIC (companions to KOIs 263, 521, 1614, and 5790). We therefore do not revise the radius estimates for the planetary candidates in these four systems and they are not included in the the following analysis.

Of the 814 planetary candidates with nearby stars detected in this survey, approximately 29% have a corrected planetary radius at least 10% larger than the original planetary radius estimate, assuming the planet candidate orbits the primary star. If instead the planet candidate orbits the secondary star which is bound to the primary star, almost every (99%) planetary candidate has a corrected radius greater than 10% larger than the original radius estimate.

If all planet candidates orbit the primary star, the original planetary radii derived from the *Kepler* light curves are underestimated by a factor of 1.08, on average. If all planet candidates instead orbit the secondary star that is bound to the primary, the corrected planetary radius estimates are on average a factor of 3.29 larger than those originally derived. The more realistic scenario is if we assume that the planet candidates are equally likely to be orbiting the primary or secondary stars. In this case, the radius estimates for the planetary candidate in systems with nearby stars will increase by a factor of 2.18 on average. This is significantly higher than the radius correction factor of 1.6 found by Ciardi et al. (2015) and 1.64 found by Hirsch et al. (2017). Hirsch et al. used planetary occurrence rates (Howard et al. 2012) to estimate the fraction of planets orbiting the primary and secondary star for known bound systems. It is unclear, however, if this approach results in a more accurate planetary correction factor estimate, because, as they note, the planet occurrence rates in binary systems is not well understood. Indeed, we found evidence in Paper III that binary stars significantly affect the properties of planetary systems, driving migration of large planets to low-period orbits.

The large number of unbound background stars likely inflates our estimates of the planetary correction radius factor. These stars are often much fainter than the primary star and the assumption that each star is equally likely to host the planet results in a large

[10] The third scenario, in which the secondary star is unbound to the primary star, is unconstrained without color information. Future papers in this survey will address the implications on the radius of *Kepler* planetary candidates in this scenario.

Table 6
Planetary Candidates Likely Not Rocky Due to Nearby Stars

Object	Sep. (″)	Δm (mag)	$R_{p,0}$[a] ($R_\oplus$)	$R_{p,\mathrm{prim.}}$[b] ($R_\oplus$)	$R_{p,\mathrm{sec.}}$[c] ($R_\oplus$)
0284.02	0.96	0.45	1.40	1.80	2.0
0284.04	0.96	0.45	1.41	1.82	2.1
0298.01	2.01	0.58	1.50	1.89	2.3
1214.01	0.33	1.21	1.44	1.66	2.4
1630.01	1.77	0.91	1.40	1.68	2.3
1700.01	0.29	1.07	1.54	1.8	2.6
1973.01	0.79	1.69	1.49	1.64	3.4
2163.03	0.77	0.04	1.59	2.23	2.2
2377.01	2.09	1.25	1.55	1.78	2.7
2486.01	0.24	0.49	1.42	1.82	2.0
2551.01	2.69	1.93	1.53	1.65	3.3
2580.01	0.60	0.86	1.59	1.92	2.5
2598.01	1.09	0.37	1.35	1.77	2.0
2711.02	0.52	0.12	1.43	1.97	2.0
2851.02	0.39	0.45	1.50	1.93	2.2
2896.02	0.96	0.38	1.57	2.05	2.3
3029.02	0.28	0.68	1.35	1.67	2.1
3112.01	1.87	0.49	1.41	1.8	2.1
3120.01	1.14	0.87	1.43	1.72	2.2
3214.01	0.49	0.73	1.53	1.88	2.2
3214.02	0.49	0.73	1.35	1.66	2.0
3435.01	3.06	1.33	1.58	1.8	2.8
3435.01	3.52	0.58	1.58	1.99	2.3
3928.01	2.96	1.21	1.45	1.67	2.3
4021.01	1.92	0.52	1.53	1.95	2.4
4323.01	1.12	2.22	1.59	1.69	3.2
4331.01	0.45	0.25	1.45	1.94	2.1
4463.01	2.45	0.01	1.52	2.14	2.1
4759.01	0.67	2.12	1.54	1.65	3.3
4823.01	1.40	0.59	1.51	1.9	2.3
5274.01	3.95	4.13	1.59	1.61	5.7
5762.01	0.23	0.65	1.37	1.71	2.2
6475.01	1.31	0.5	1.54	1.97	2.3
6482.01	0.52	0.58	1.53	1.93	2.4
6907.01	3.35	−0.36	1.14	1.76	1.6

Notes.
[a] Original planetary radius estimate, from NASA Exoplanet Archive.
[b] Estimated planetary radius in the scenario where the planet orbits the target star, irregardless whether the secondary star is bound or unbound to the target star.
[c] Estimated planetary radius in the scenario where the planet orbits the secondary star, which is physically bound to the target star.

number of gas giant planets, which are inherently rare compared to terrestrial planets (Howard et al. 2012). Simulations from galactic stellar models suggest that the majority of nearby stars to KOIs at separations larger than 1″ are likely unbound (Horch et al. 2014), a conclusion borne out by observations (Atkinson et al. 2017; Hirsch et al. 2017). If we limit our survey to just those likely bound nearby stars within 1″, we find radius correction factors of 1.18, 1.88, and 1.54 for the scenarios where all planets orbit the primary star, all planets orbit a bound secondary star, and all planets are equally likely to orbit either star, respectively. The radius correction factors found for the set of likely bound stars is in agreement with that found by Hirsch et al. (2017), and is our recommended estimate for the true radius correction factor for *Kepler* planetary candidates with detected nearby stars. We will quantify the probability of association for every detected nearby star in future papers in this survey, allowing us to better remove unbound background stars from our sample and revisit this discussion.

Lastly, using the original estimates for planetary radius and the planetary radius ranges listed in Table 5, we find the radius correction factor for systems with nearby stars within 4″ (1″) for Earth-sized planets is 2.30 (1.54), for Neptune-sized planets is 2.25 (1.59), for Saturn-sized planets is 1.95 (1.67), and for Jupiter-sized planets is 1.88 (1.38), if we assume that each nearby star is bound and the planetary candidate is equally likely to orbit the primary or secondary star. Under these same assumptions, we estimate that approximately 140 previously believed rocky planet candidates ($R_{p,0} < 1.6\,R_\oplus$), or 9% of the 1480 rocky planet candidates discovered by *Kepler*, have corrected radii larger than the rocky planet cut-off at $1.6R_\oplus$ as described in Rogers (2015) due to nearby stars within 4″. These 140 planetary candidates are therefore likely not rocky due to incorrect identification of the planetary host star and photometric contamination from nearby stars.

We also find 35 rocky planet candidates that, due to the presence of a previously undetected nearby star, are now likely not rocky if either orbiting the primary or secondary stars. We highlight these planetary candidates in Table 6.

5.3. Rocky, Habitable Zone Candidates

A primary objective of the *Kepler* mission was to estimate $\eta_\oplus$, the occurrence rate of Earth-like planets orbiting in the habitable zone. Contamination from nearby stars has a significant effect on the derived planetary radii. Planetary radii based on *Kepler* light curves alone are underestimated by a factor of approximately 1.5 on average, as discussed in Section 5.2. The impact of nearby stars must, therefore, be taken into account to estimate precisely what planets are terrestrial. While the exact requirements for habitability remain unclear (Kasting et al. 1993; Selsis et al. 2007; Seager 2013; Zsom et al. 2013), it is believed that the equilibrium temperature of the planet must allow the presence of liquid water. To be Earth-like, a planet must also be rocky: Rogers (2015) show that the transition between "rocky" and "non-rocky" occurs rather sharply at $R_P = 1.6\,R_\oplus$.

We searched for potentially rocky planets, with estimated radii less than 2σ away from the rocky planet cut-off of $1.6R_\oplus$, residing in the habitable zone (estimated planetary equilibrium temperature $\leqslant$370 K) within the set of systems with newly discovered nearby stars. We find three such planetary candidates, detailed in full in Appendix B and highlighted in Table 7.

The two confirmed planets, KOI-701.03 and 701.04 (Kepler-62e and Kepler-62f, respectively), both reside in the habitable zone if orbiting the primary star. If instead, either one orbits the faint secondary star and that star is bound to the primary, the estimated radii of each would be much larger and it would be unlikely that they would be rocky in composition. This planet has been thoroughly vetted by Borucki et al. (2013), who concluded that the two planets are indeed rocky and orbit in the habitable zone.

KOI-7470.01 has an original radius estimate of $1.9R_\oplus$, near the rocky planet cut-off, and an estimated equilibrium temperature of 225 K. The undiluted radius estimate for the scenario where the planetary candidate orbits the primary is $2.59R_\oplus$, making it very improbable that the planet is rocky. Likewise, if the planetary candidate instead orbits the bound secondary star, it would again be unlikely to be rocky, with a planetary radius estimate of $2.70R_\oplus$.

Table 7
Implications on Derived Radius of Potentially Rocky, Habitable Zone Planets

Object	Equil. Temp.[a] (K)	$R_{p,0}$[b] ($R_\oplus$)	$R_{p,\mathrm{prim.}}$[c] ($R_\oplus$)	$R_{p,\mathrm{sec.}}$[d] ($R_\oplus$)
0701.03	269	1.72	1.73	10.94
0701.04	207	1.43	1.44	9.1
7470.01	225	1.9	2.59	2.67

Notes.
[a] Estimated planetary equilibrium temperature, from NASA Exoplanet Archive.
[b] Original planetary radius estimate, from NASA Exoplanet Archive.
[c] Estimated planetary radius in the scenario where the planet orbits the target star.
[d] Estimated planetary radius in the scenario where the planet orbits the secondary star, which is physically bound to the target star.

6. Conclusion

Combining the data sets from the complete Robo-AO KOI survey, we found 610 nearby stars around 559 planetary candidate hosts, from a target list of 3857 KOIs, implying a nearby star fraction rate of 14.5% ± 0.6% within the Robo-AO detectability range (separations between ∼0.″15 and 4.″0 and $\Delta m \leqslant 6$). We found a nearby star fraction for Earth-sized planets of 16.3 ± 1.0%, for Neptune-sized planets of 13.0 ± 0.8%, for Saturn-sized planets of 13.6 ± 2.0%, and for Jupiter-sized planets of 19.0 ± 2.8%. We derived the corrected planetary radius for every planetary candidate with nearby stars in this survey. We found that planets in systems with likely bound nearby stars have underestimated radii by a factor of 1.54, assuming that each planet is equally likely to orbit the primary or secondary star. We found that 35 of the previously believed rocky planet candidates detected by *Kepler* are likely not rocky due to the presence of a nearby star.

We have also recently made the results of our survey available at a survey website.[11]

In future papers in this analysis, we will use the nearly 4000 high-resolution images of planetary candidate hosts to search for insight into the how binary stars impact planetary formation and evolution. In 2017, we began a campaign to characterize the detected nearby stars to planetary candidate hosts with multi-band photometry. This study will allow the probability of association between stars in each system to be quantified. We are also studying the potential of AO transit observations to detect the source of the transit signal in multiple star systems. While the transit of many *Kepler* planets will likely be too shallow to detect with Robo-AO, we could detect deeper transits from background eclipsing binaries that, when blended with the bright primary stars, are the source of false positive planetary transit signals.

A second generation Robo-AO instrument on the University of Hawai'i 2.2 m telescope on Maunakea (Baranec et al. 2014a) is being built. The Kitt Peak and Maunakea systems will together image up to ∼500 objects per night and have access to three-quarters of the sky over the course of a year. A southern analog to Robo-AO mounted on the Southern Astrophysical Research Telescope at CTIO and capable of twice *HST* resolution imaging, is also in development (Ziegler et al. 2016). With unmatched efficiency, Robo-AO and its lineage of instruments are uniquely able to perform high-acuity imaging of the hundreds of K2 (Howell et al. 2014) planetary candidates, ground-based transit surveys such as MEarth (Nutzman & Charbonneau 2008), KELT (Pepper et al. 2007, 2012), HATNet (Bakos et al. 2004), SuperWASP (Pollacco et al. 2006), NGTS (Wheatley et al. 2013), XO (McCullough et al. 2005), and the Evryscope (Law et al. 2015), as well as the thousands of expected exoplanet hosts discovered by the forthcoming NASA Transiting Exoplanet Survey Satellite (Ricker et al. 2015) and ESA PLAnetary Transits and Oscillations of stars 2.0 (Rauer et al. 2014) missions.

We thank the anonymous referee for careful analysis and useful comments on the manuscript.

This research is supported by the NASA Exoplanets Research Program, grant #NNX 15AC91G. C.Z. and W.H. acknowledge support from the North Carolina Space Grant consortium. C.B. acknowledges support from the Alfred P. Sloan Foundation.

The Robo-AO team thanks NSF and NOAO for making the Kitt Peak 2.1 m telescope available. We thank the observatory staff at Kitt Peak for their efforts to assist Robo-AO KP operations. Robo-AO KP is a partnership between the California Institute of Technology, the University of Hawaii, the University of North Carolina at Chapel Hill, the Inter-University Centre for Astronomy and Astrophysics (IUCAA) at Pune, India, and the National Central University, Taiwan. The Murty family feels very happy to have added a small value to this important project. Robo-AO KP is also supported by grants from the John Templeton Foundation and the Mt. Cuba Astronomical Foundation. The Robo-AO instrument was developed with support from the National Science Foundation under grants AST-0906060, AST-0960343, and AST-1207891, IUCAA, the Mt. Cuba Astronomical Foundation, and by a gift from Samuel Oschin. These data are based on observations at Kitt Peak National Observatory, National Optical Astronomy Observatory (NOAO Prop. ID: 15B-3001), which is operated by the Association of Universities for Research in Astronomy (AURA) under cooperative agreement with the National Science Foundation.

This research has made use of the Exoplanet Follow-up Observation Program website, which is operated by the California Institute of Technology, under contract with the National Aeronautics and Space Administration under the Exoplanet Exploration Program

This research has made use of the NASA Exoplanet Archive, which is operated by the California Institute of Technology, under contract with the National Aeronautics and Space Administration under the Exoplanet Exploration Program.

Facilities: PO:1.5 m (Robo-AO), KPNO:2.1 m (Robo-AO).

Appendix A
PSF Subtraction Collisions

By using other Robo-AO observations of KOIs as reference images, there is a possibility that an image used as a reference PSF will have a nearby star at a similar position with respect to its host star as the image being modeled. Only companions at separations less than 1″ could potentially avoid detection by both our visual search and the automated companion detection routine. Such a scenario (a "collision") could lead to real companions being removed from target images if they coincide with a reference star's companion. To estimate how near to each other the companions must be for a collision to

[11] http://roboaokepler.org/

Table 8
Implications on Derived Radius of *Kepler* Planetary Candidates

Object	Sep. (″)	Δm (mag)	Reference[a]	$R_{\star,\mathrm{target}}$[b] ($R_\odot$)	$R_{\star,\mathrm{secondary}}$[c] ($R_\odot$)	$R_{p,0}$[d] ($R_\oplus$)	$R_{p,\mathrm{prim.}}$[e] ($R_\oplus$)	$R_{p,\mathrm{sec.}}$[f] ($R_\oplus$)
0001.01	1.13	3.95	P1	0.96	0.58	13.0	13.2	49.1
0004.01	3.42	4.46	P2	2.99	0.58	12.9	13.0	19.8
0013.01	1.16	0.19	P1	3.03	2.58	21.4	29.1	36.1
0042.01	1.74	3.04	P2	1.34	0.75	2.43	2.5	5.7
0044.01	3.42	4.03	TW	1.07	0.6	12.0	12.1	43.5

Notes.
[a] Reference for nearby star detection: (P1, Law et al. 2014), (P2, Baranec et al. 2016), (P3, Ziegler et al. 2017), (TW, this work).
[b] Primary stellar radius estimate from Mathur et al. (2017).
[c] Estimated radius of secondary stellar companion in the scenario where it is bound to the primary star, using absolute magnitude difference in the *Kepler* band and the Dartmouth stellar models (Dotter et al. 2008).
[d] Original planetary radius estimate, from NASA Exoplanet Archive.
[e] Estimated eclipsing object radius in the scenario where it is physically bound to the target star, corrected for transit dilution caused by the presence of either bound or unbound nearby stars.
[f] Estimated eclipsing object radius in the scenario where it is bound to the companion star, correcting for transit dilution by nearby stars and using the stellar radius estimate of the companion in this table.

(This table is available in its entirety in machine-readable form.)

Table 9
Full Robo-AO Observation List

KOI	m_{Kep} (mag)	UT Date	Obs. Qual.	Comp. Det.?
K019	11.37	2016 Jun 14	medium	⋯
K025	13.5	2016 Jul 08	medium	⋯
K048	13.72	2016 Jun 25	low	⋯
K072	10.96	2016 Jul 02	high	⋯
K0120	12.0	2016 Jul 15	medium	yes

(This table is available in its entirety in machine-readable form.)

occur, we ran the PSF subtraction routine on a set of 10 targets that have detected nearby stars at varying separations within 1″. We then include a copy of each target image as one of the reference PSFs. In each case, the nearby star is not detected in the subtracted image by eye or by the automated companion detection routine with a significance $>3\sigma$. The reference image is then rotated by two degrees, and the PSF subtraction routine is rerun. This process is iterated until the nearby star is able to be detected in the subtracted image. We find on average the companion in the reference image must be within 0.″05 of the position of the nearby star in the original image for a collision to occur.

To estimate the expected number of collisions in our analysis, we use the observed distribution of nearby stars from our survey to populate a simulated KOI survey. For each nearby star detected with separations less than 1″, we randomly drew 20 other reference stars. We counted every time a reference star fell within 0.″05 of the original star as a collision. With 100 simulations performed, we estimate the number of expected companions missed in our survey due to collisions is 0.44 ± 0.18, or approximately one every two surveys.

The visual search for companions, however, will greatly reduce the number of expected companions missed in our analysis. Within our observations, we find two potential collisions (KOIs 3497 and 4098, and KOIs 6202 and 6602). Neither of these sets of colliding images were used as a reference image for each other in the initial data analysis. We reran the PSF subtraction routine for both sets using the colliding system for each as a reference image. In each case, the nearby star is only partially subtracted and is still detectable within the subtracted image. This suggests that slight alterations in the Robo-AO PSFs are sufficient to effectively eliminate the possibility that a real companion will be erroneously subtracted off by the PSF subtraction routine.

Appendix B
Updated Planetary Radii

In Table 8, we derive the corrected planetary radii for every *Kepler* planetary candidate with a detected nearby star (as described in Section 5.2).

Appendix C
Full Robo-AO Observations Table

In Table 9, we list KOIs observed with Robo-AO at Kitt Peak, including the date the target was observed, observation quality (as described in Section 3.5), and the presence of detected companions.

ORCID iDs

Carl Ziegler https://orcid.org/0000-0002-0619-7639
Nicholas M. Law https://orcid.org/0000-0001-9380-6457
Christoph Baranec https://orcid.org/0000-0002-1917-9157
Reed Riddle https://orcid.org/0000-0002-0387-370X
Dmitry A. Duev https://orcid.org/0000-0001-5060-8733
Rebecca Jensen-Clem https://orcid.org/0000-0003-0054-2953
S. R. Kulkarni https://orcid.org/0000-0001-5390-8563
Tim Morton https://orcid.org/0000-0002-8537-5711
Maïssa Salama https://orcid.org/0000-0002-5082-6332

References

Adams, E. R., Ciardi, D. R., Dupree, A. K., et al. 2012, AJ, 144, 42
Adams, E. R., Dupree, A. K., Kulesa, C., & McCarthy, D. 2013, AJ, 146, 9
Atkinson, D., Baranec, C., Ziegler, C., et al. 2017, AJ, 153, 25

Bakos, G., Noyes, R. W., Kovács, G., et al. 2004, PASP, 116, 266
Baranec, C., Riddle, R., Law, N. M., et al. 2013, Journal of Visualized Experiments, 72, e50021
Baranec, C., Riddle, R., Law, N. M., et al. 2014a, Proc. SPIE, 9148, 91481D
Baranec, C., Riddle, R., Law, N. M., et al. 2014b, ApJL, 790, L8
Baranec, C., Ziegler, C., Law, N. M., et al. 2016, AJ, 152, 18
Batalha, N. M., Rowe, J. F., Bryson, S. T., et al. 2013, ApJS, 204, 24
Borucki, W. J., Agol, E., Fressin, F., et al. 2013, Sci, 340, 587
Borucki, W. J., Koch, D. G., Basri, G., et al. 2011a, ApJ, 728, 117
Borucki, W. J., Koch, D. G., Basri, G., et al. 2011b, ApJ, 736, 19
Borucki, W. J., Koch, D. G., Brown, T. M., et al. 2010, ApJL, 713, L126
Burgasser, A. J., Kirkpatrick, J. D., Reid, I. N., et al. 2003, ApJ, 586, 512
Burke, C. J., Bryson, S. T., Mullally, F., et al. 2014, ApJS, 210, 19
Ciardi, D. R., Beichman, C. A., Horch, E. P., & Howell, S. B. 2015, ApJ, 805, 16
Coughlin, J. L., Mullally, F., Thompson, S. E., et al. 2016, ApJS, 224, 12
Dotter, A., Chaboyer, B., Jevremović, D., et al. 2008, ApJS, 178, 89
Dressing, C. D., Adams, E. R., Dupree, A. K., Kulesa, C., & McCarthy, D. 2014, AJ, 148, 78
Dressing, C. D., & Charbonneau, D. 2013, ApJ, 767, 95
Duquennoy, A., & Mayor, M. 1991, A&A, 248, 485
Evans, D. F., Southworth, J., Maxted, P. F. L., et al. 2016, A&A, 589, A58
Everett, M. E., Barclay, T., Ciardi, D. R., et al. 2015, AJ, 149, 55
Fabrycky, D., & Tremaine, S. 2007, ApJ, 669, 1298
Fressin, F., Torres, G., Charbonneau, D., et al. 2013, ApJ, 766, 81
Fruchter, A. S., & Hook, R. N. 2002, PASP, 114, 144
Furlan, E., Ciardi, D. R., Everett, M. E., et al. 2017, AJ, 153, 71
Gilliland, R. L., Cartier, K. M. S., Adams, E. R., et al. 2015, AJ, 149, 24
Haas, M. R., Batalha, N. M., Bryson, S. T., et al. 2010, ApJL, 713, L115
Hirsch, L. A., Ciardi, D. R., Howard, A. W., et al. 2017, AJ, 153, 117
Horch, E. P., Howell, S. B., Everett, M. E., & Ciardi, D. R. 2012, AJ, 144, 165
Horch, E. P., Howell, S. B., Everett, M. E., & Ciardi, D. R. 2014, ApJ, 795, 60
Howard, A. W., Marcy, G. W., Bryson, S. T., et al. 2012, ApJS, 201, 15
Howell, S. B., Everett, M. E., Sherry, W., Horch, E., & Ciardi, D. R. 2011, AJ, 142, 19
Howell, S. B., Sobeck, C., Haas, M., et al. 2014, PASP, 126, 398
Jensen-Clem, R., Duev, D. A., Riddle, R., et al. 2018, AJ, 155, 32
Kasting, J. F., Whitmire, D. P., & Reynolds, R. T. 1993, Icar, 101, 108
Kraus, A. L., Ireland, M. J., Huber, D., Mann, A. W., & Dupuy, T. J. 2016, AJ, 152, 8
Lafrenière, D., Marois, C., Doyon, R., Nadeau, D., & Artigau, É 2007, ApJ, 660, 770
Law, N. M., Fors, O., Ratzloff, J., et al. 2015, PASP, 127, 234
Law, N. M., Mackay, C. D., Dekany, R. G., et al. 2009, ApJ, 692, 924
Law, N. M., Morton, T., Baranec, C., et al. 2014, ApJ, 791, 35
Lawrence, A., Warren, S. J., Almaini, O., et al. 2007, MNRAS, 379, 1599
Lillo-Box, J., Barrado, D., & Bouy, H. 2012, A&A, 546, A10
Lillo-Box, J., Barrado, D., & Bouy, H. 2014, A&A, 566, A103
Marcy, G. W., Isaacson, H., Howard, A. W., et al. 2014, ApJS, 210, 20
Mathur, S., Huber, D., Batalha, N. M., et al. 2017, ApJS, 229, 30
McCullough, P. R., Stys, J. E., Valenti, J. A., et al. 2005, PASP, 117, 783
Morton, T. D., Bryson, S. T., Coughlin, J. L., et al. 2016, ApJ, 822, 86
Morton, T. D., & Johnson, J. A. 2011, ApJ, 738, 170
Naoz, S., Farr, W. M., & Rasio, F. A. 2012, ApJL, 754, L36
Ngo, H., Knutson, H. A., Hinkley, S., et al. 2016, ApJ, 827, 8
Nutzman, P., & Charbonneau, D. 2008, PASP, 120, 317
Pepper, J., Kuhn, R. B., Siverd, R., James, D., & Stassun, K. 2012, PASP, 124, 230
Pepper, J., Pogge, R. W., DePoy, D. L., et al. 2007, PASP, 119, 923
Petrovich, C. 2015, ApJ, 799, 27
Pollacco, D. L., Skillen, I., Collier Cameron, A., et al. 2006, PASP, 118, 1407
Raghavan, D., McAlister, H. A., Henry, T. J., et al. 2010, ApJS, 190, 1
Rasio, F. A., & Ford, E. B. 1996, Sci, 274, 954
Rauer, H., Catala, C., Aerts, C., et al. 2014, ExA, 38, 249
Ricker, G. R., Winn, J. N., Vanderspek, R., et al. 2015, JATIS, 1, 014003
Riddle, R. L., Burse, M. P., Law, N. M., et al. 2012, Proc. SPIE, 8447, 84472O
Rogers, L. A. 2015, ApJ, 801, 41
Rowe, J. F., Bryson, S. T., Marcy, G. W., et al. 2014, ApJ, 784, 45
Santerne, A., Fressin, F., Díaz, R. F., et al. 2013, A&A, 557, A139
Seager, S. 2013, Sci, 340, 577
Selsis, F., Kasting, J. F., Levrard, B., et al. 2007, A&A, 476, 1373
Torres, G., Kipping, D. M., Fressin, F., et al. 2015, ApJ, 800, 99
Wang, J., Fischer, D. A., Horch, E. P., & Xie, J.-W. 2015a, ApJ, 806, 248
Wang, J., Fischer, D. A., Xie, J.-W., & Ciardi, D. R. 2014, ApJ, 791, 111
Wang, J., Fischer, D. A., Xie, J.-W., & Ciardi, D. R. 2015b, ApJ, 813, 130
Wheatley, P. J., Pollacco, D. L., Queloz, D., et al. 2013, European Physical Journal Web of Conferences, 47, 13002
Ziegler, C., Law, N. M., Morton, T., et al. 2017, AJ, 153, 66
Ziegler, C., Law, N. M., & Tokovinin, A. 2016, Proc. SPIE, 9909, 99093Z
Zsom, A., Seager, S., de Wit, J., & Stamenković, V. 2013, ApJ, 778, 109